International Journal for Housing Science and Its Applications
Publish August 4, 2025. Volume 46, Issue 3 Pages 2402-2413

https://doi.org/10.70517/ijhsa463201

Research on surface movement and deformation law under repeated mining conditions

Dongdong Zhang[1,*], Xueyi Yu[2] and Junjie Liu[2]
[1] Shaanxi Energy Institute, Xianyang, Shaanxi, 712000, China
[2] Xi'an University of Science and Technology, Xi'an, Shaanxi, 710054, China
Corresponding authors: (e-mail: xust_zhangdd0629@163.com).

Abstract This study is to further explore the influence of repeated mining on surface changes in coal mining areas, and discuss the law of surface movement under special surface conditions. Based on the observation technology of surface movement and the numerical simulation method of universal discrete element code (UDEC), it analyzes the surface movement of mining surfaces 204 and 205 in the panel 2 area of Tingnan Coal Mine in Binchang mining area under repeated mining. The research results show that the 204 working area is extremely inadequately mined, so the surface movement is very small, the subsidence rate is only 0.046, and the surface deformation is weak, which will not cause damage to the surface construction facilities. The mining results in the 205 working area, which is close to the conventional full mining conditions, show that the surface movement is serious with obvious deformation, and the subsidence rate reaches 0.22, which is far from the maximum subsidence value, and the insufficient mining subsidence range shows basically same with that of the sufficient mining. Simultaneously, the surface movement law of multi-face mining is simulated based on the UDEC numerical simulation method. The results reveal that the mining surface movement law of 204 and 205 working faces is basically consistent with the surface observation results. The content of this study can provide scientific and effective reference materials for subsequent research on surface movement monitoring, and is of great significance to the safe mining of coal under buildings (structures) in Binchang mining area.

Index Terms surface movement monitoring, repeated mining, coal mine, surface change

I. Introduction

With the increasing demand for energy in society, China' coal mining industry is booming. In some resource-intensive areas, the coal industry has also contributed a lot to the economic development of the area [1]. While bringing huge economic benefits, the coal industry also causes some harms to the environment and geology, which can't be ignored [2]. Especially under the construction of a resource-friendly development model in China, it is necessary to pay more attention to the environmental impact of coal mining [3]. According to data, the total amount of coal under the buildings, under the railways, and under the water-bodies ("three unders") exceeds 13.3 billion tons, of which 7.82 billion tons of coal are under the buildings, accounting for 61% of the total coal of the "three unders". In addition, almost every mine faces the coal under buildings [4], [5]. With the depletion of easy-to-mine coal resources in mining areas and the increase in demand for coal in related industries, the "three unders" of mining are imminent [6]. In addition to the safe and reasonable mining of coal resources, the mining of "three unders" coals have to also avoid the deformation of surface movement that will cause great impact or even damage to buildings, railways, and water bodies [7]. The premise to solve these problems is to study the deformation law of surface movement after mining.

At this stage, the main mining method of coal mines in China is the fully mechanized mining method, but in some areas where the thickness of the coal seam is not very large, the method of mining the full height at one time is generally selected [8]. This method shows the advantages of high mining efficiency and good recovery rate. However, it is very easy to cause the overlying rock stress to redistribute on the working face, and the overlying rock mass to develop fissures, and sometimes even harm the surface due to the particularity of full height mining at one time [9], [10]. Therefore, it is necessary to monitor the movement and state of the ground surface [11]. Under the background of this era, automatic surface observation technology has been fully developed and applied [12]. In the application of surface movement monitoring, the form of surface movement observation station is mainly used [13]. Based on the analysis of the surface movement observation station data, it can not only draw the law of movement and destruction of the surface after coal mining, lay a technical basis for the overall planning of the mining area, but also provide data for the adjustment of underground mining technology [14].

The Tingnan Coal Mine located in the southwest of Tingkou Town in Changwu County of Shaanxi Province is selected as the research object. Based on surface movement monitoring, the relevant laws of surface mining in working areas 204 and 205 in the panel 2 of the coal mine are explored, so as to obtain the related parameters on surface movement of 204 and 205 working areas. In addition, a surface simulation movement experiment is carried out on the 204 and 205 working areas based on the numerical simulation method. This study aims to analyze the influences of repeated mining on these two working areas more clearly and contribute to the construction of Tingnan Coal Mine.

II. Methods

II. A. Introduction of the research area

(1) Geographical location

The research area in this study is Tingnan Coal Mine in Tingkou Town in Changwu County of Xianyang City of Shaanxi Province. The area where the coal mine is located has convenient transportation. The National Highway 312 passes through the east of the minefield. It is also close to the Fuzhou-Yinchuan Expressway and the Xi'an-Pingliang Railway, which provides convenience for coal transportation [15]. The region where Tingnan Coal Mine is located is a coal mine gathering area. It is adjacent to Mengcun Coal Mine and Dafosi Coal Mine in south, Yangjiaping Coal Mine in west, Xiaozhuang Coal Mine in east. The entire mine field is about 11.3 km long from east to west, 5.1 km wide from north to south, with an area of 35.5484 km2. Its mining elevation is +530 ~ +350 meters. The mine field belongs to the landform of Yuanchuan, with high west and low east. The plateau is open and flat, the highest elevation is +1194 meters, the lowest elevation is +850 meters, and the maximum elevation difference of the plateau is 344 meters. The elevation of the main shaft of the mine is +856.30 meters, and the elevation of the auxiliary shaft is +856.35 meters. The highest flood level in the past years was +851.70 meters, and the mine is not threatened by floods.

At this stage, Tingnan Coal Mine includes 4 panels: the working faces 101, 103, 106, 107, 109, 111, and 113 have been mined in panel 1; the working faces 201, 204, and 205 have been mined in panel 2; the working face 303 has been mined and 304 is recovering. In this study, 204 and 205 the panel 2 have been investigated in this study.

(2) Structure and rock mechanical properties

The bottom structure of panel 2 in this research area mainly includes the following types: Triassic, Jurassic, Cretaceous, Neogene, and Quaternary [16], [17]. Among them, the Triassic system is only distributed in the Hujiacun Formation, the geological lithology of which is gray, dark gray mudstone, siltstone mixed with gray-green medium-thick layered medium-fine feldspar sandstone. The mudstone of this series is pure and fine, with well-developed horizontal bedding, and becomes thin slices after weathering. Sandstone is cemented tightly, with uniform bedding and wavy bedding. The maximum drilling thickness of this system is 61.10 meters. It is mainly a coal-bearing sedimentary basement. Its top surface is undulating. After being filled and supplemented by the Fuxian Formation of the Lower Jurassic, it creates favorable conditions for the deposition of coal seams in the Yan'an Formation.

The thickness of the rock pillars in the panel 2 of the Jurassic is 99.35 ~ 153.84 meters, of which the thickness of mudstone-like rock layers is 12.03 ~125.05 meters, the average thickness is 62.3 mm, and the proportion of rock pillars is 10.4~81.3%, which accounts for 46.9% in average; the thickness of the sandstone layer is 28.79 ~ 112.4 meters, the average thickness is 83.7 meters, the proportion of rock pillars is 18.7~89.6%, accounting for 53.1% in average. Whether it is the upper Anding Formation or the Zhiluo Formation in the middle, it is almost always a rock structure with a soft and hard interactive structure. In the upper Anding Formation, the thickness of a single layer of soft rock is relatively large, while that of sandstone is relatively large. The thickness of the three layers of mudstone is above 10 meters, and the maximum thickness reaches 17.3 meters. Jurassic rock formations are not exposed in the area, but only in the Shuiliangou, Huoshizui and Baizigou areas east of Binxian outside the area.

The Cretaceous rock section is composed of the Yijun, Luohe, and Huachi formations. The lithology and thickness of the three are quite different, and the thickness is dominated by the sandstone of the Luohe formation. The Yijun Formation has a single lithology, mainly conglomerate-like rock formations, with a few drill holes showing sandstone with hard lithology. The average thickness is 32.87 meters. The rock layers of the Luohe Formation are composed of sandstone, conglomerate and mudstone, mainly sandstone. The sandstone of the Luohe Formation is thick, strong, and widely distributed. According to the drilling results of the panel 2, the thickness of the Luohe Formation is 231.46 ~ 312.8 mm, and the average thickness is 290.68 mm. The average thickness of sandstone-like rock layers is 228.28 mm, accounting for 78.53% on average, and the average thickness of conglomerate-like rock layers is 46.69 mm, accounting for 16.06% on average. The average thickness of mudstone-like rock layers is 15.71 mm, accounting for an average of 5.40%. The Huachi Formation is mainly composed of mudstone and sandstone, mainly

mudstone. The cumulative thickness is 0 ~ 60.17 mm, the distribution is uneven, and the rock and soil of this group are missing in some boreholes.

The loose layers of Neogene and Quaternary are mainly quicksand-silt layer formation, sand-pebble layer formation, loess layer formation, and clay layer formation. The cumulative thickness is uneven (0.5 ~ 209 mm), and the thickness of the loose layer is small at the bank and gully slope, and that on the plateau surface is large. The quicksand-silt layer group is distributed in the Jinghe, Heihe, and other large river valleys, and is the accumulation of the Quaternary Holocene river floodplain. The sand and gravel layer group is distributed in the Jinghe, Heihe, and other large river valleys, and is the sediment of the Quaternary Holocene riverbed. The loess layer group is distributed in the loess plateau area, including the Quaternary Middle Pleistocene Lishi loess and Upper Pleistocene Malan loess. Malan loess is mainly silt, loose, with large pores, well-developed vertical joints, and good water permeability. Lishi loess is sub-sandy soil, loam, and paleosol interbedded, the upper structure is loose, porous, containing irregular calcareous nodules, and the lower part is dense, with few and small pores, th multiple layers of calcareous nodules. The clay layer group includes Neogene red clay and Quaternary Lower Pleistocene Wucheng loess. The lithology is mainly clay, loam, and sand-bearing clay, with calcareous nodules and no collapsibility.

(3) Topography

The surface of the panel 2 is a loess plateau landform, and the ravine is severely cut [18]. The quaternary loess is covered with normal vegetation conditions [19]. The Heihe River flows through the mining face corresponding to the middle and northern part of the surface, where the Cretaceous Luohe and Huachi formations are exposed. The loose layer of the Heihe river bed has a small thickness and small variation, ranging from 0 to 0.5m. The loose layer on both sides of the cliffs has a large thickness and variation. The loess layer in some areas is thicker than 100 mm, which is a huge loess layer. The surface structures in the second panel area mainly include the Tingkou Reservoir dam and its auxiliary facilities, which mainly include flood discharge tunnels, water conveyance tunnels, and spillways. The annex buildings of Tingkou Reservoir and the three administrative villages, which are Yujiashan Village, Yangpo Village, and Yangchang Village. Only the villages and the Heihe river beach are relatively flat, while other sections have large fluctuations and surface slope changes.

(4) Working area overview

Mining Jurassic No. 4 coal seam in panel 2 is a single coal seam. Except for the thinning layer in the northwest, other areas are relatively stable, with a thickness of 0.8 ~ 20.46 meters and an average thickness of 15.03 meters; the inclination of the coal seam is 2° ~ 4°, the average inclination angle is 3°; generally, there are 1 to 4 layers of gangue in the upper part, the thickness of the gangue is small (0.06 ~ 1.0 meter), with an average of 0.40 meters. The gangue lithology is mudstone and carbonaceous mudstone. The seam elevation is +398 ~ +460 meters, and the ground elevation is +849.2 ~ +1124.2 meters.

There are 204, 205, 206, and 207 working faces in the panel 2 from east to west. Among them, 204 and 205 working faces have been stopped, and 206 working face is currently working. The 204 working face is located in the northeast of the mine, with a north-south direction and a working face length of 200 meters. The Heihe River flows directly above the north of the working face twice. The thickness of the coal seam on this face is 16.9 ~ 21.0 meter, with an average of 19.1 meters, and the coal seam inclination is 0°-5°. The 205 working face is located in the west of the 204 working face in the panel 2, and the working face length is 200 meters. The minable part of the working face is about 360 meters from the south end to the north to the position of the cut hole under the Heihe river bed, and the terrain is relatively flat. The coal seam thickness of 205 working face is 16.5 ~ 20.2 meters, with an average of 18.35 meters, the coal seam inclination is 0°-6°, and the geological structure is simple. 205 is the replacement working face of 204, and there are coal pillars of 30 meters between the working faces. The 204 and 205 working faces adopt layered fully mechanized mining method, and the layered mining thickness is 5 ~ 6 meters. 206 is the replacement working face of 205. The length of 206 working face is 200 meters. The designed average mining height is 7.5 meters. The buried depth of the coal seam is 456 ~ 694 meters. The fully mechanized top coal caving mining technology is adopted for mining, with a recoverable reserve of 3.6 million tons.

II. B. Design on observation technology of surface movement

The following principles should be followed when the observation line is set. Firstly, the position of the observation line should be on the main influence line of the surface subsidence range [20]. Secondly, the observation line is not affected by nearby mining during the observation period [21]. Besides, the observation range of the observation line should not be less than the surface subsidence area [22]. In addition, the density of measuring points in the observation station should be appropriate to ensure the reliability of the data and minimize the cost of measuring points [23]. Finally, the reference point of the observation station should be placed outside the influence range of the surface subsidence area to ensure that it is not affected by underground mining activities [24].

The ground surface of the research area is mainly loess plateau landform, the landform environment is interlaced with gully, the terrain is complex, and there are rivers flowing through, so it is more necessary to arrange the observation points reasonably [25]. Based on the basic principles of the above observation line design, the observation lines and observation points are set in the research area. The observation line design of this study mainly includes the A, B, and C, which are all unconventional observation lines. It firstly considers the arrangement of two vertical and intersecting observation lines C and B along the strike main section and the inclined main section of the research area 204. Since observation points (Heihe, river beach, and cliffs) can't be buried in some locations within the distance affected by mining in the northern part of the cut eye, the design of the towards observation line C can only be to bury 8 observation points (namely C1 ~ C8) at the 275 meters in south of the cut eye, with a length of 175 meters and the measuring point spacing of 30 meters. Affected by the surface topography and the Heihe River, the oblique observation line B can't be arranged according to the main section of the inclination. It is considered comprehensively to arrange it along the steep slope of the northern face of the working face, but the length of the arrangement can only be observed in the semi-basin on the side of the 204 working face. Line B is 175 ~ 487 meters away from the 204 working face, with a projection length of 784 meters along the oblique direction. A total of 31 observation points (B1 ~ B31) are arranged, and the observation point spacing is 30 meters. Observation line A is located at the end of the cut eye of the 205 working face, perpendicular to the advancing direction of the working face. The cut-off cut of line A is 300 meters away from the 205 working face, and the projection length is 840 meters along the oblique direction. A total of 27 measuring points (A1 ~ A27) are arranged, and the distance among the measuring points is 30 meters. After the 206 working face is mined, the observation line A has been adjusted by adding conventional points A28 ~ A35 and control points AA1 ~ AA3 to expand the observation range.

II. C. Design on related parameters for observation technology of surface movement

(1) Affecting area of mining

Based on the stratigraphic structure and rock mechanical properties of the panel 2, the surface observation achievements of 101 ~ 103 and 109 ~ 113 working faces of the Tingnan Mine with large and deep working area, the surface observation achievements of 107 working face under extremely inadequate mining, and the surface observation results of adjacent Xiagou mine, the surface movement angle parameter is adopted for designing the observation lines to predict the mining influence range and determine the observation line in consideration of that the Luohe Group sandstone is 300 meters thickness in the upper coal seam, so as to determine the length and position of the observation line. The specific contents are shown in Table 1 below, which reveals that the strike movement angle δ is 75°, the uphill movement angle γ is 75°; the downhill movement angle β is 75°; the loose layer movement angle φ is 45° in the parameter design.

Table 1: Related angle parameters of surface movement

Type	Angle
Strike shift angle (δ)	75°
Uphill movement angle (γ)	75°
Downhill mountain angle (β)	75°
Loose layer movement angle (φ)	45°

The mining influence distance can be obtained based on the loose layer movement angle, strike movement angle, and the depth of mining at the opening cut of the working face, as follows:

$$L_{trend} = h\cot\varphi + (H_0 - h)\cot(\delta - \Delta\delta) \quad (1)$$

In the above equation, h is the thickness of the loose layer; φ is the loose layer movement angle; H_0 refers to the mining depth of the open cut (or stop line) of the working face; δ is the strike movement angle; and $\Delta\delta$ is the correction value of the strike movement angle.

The inclination direction can be determined according to the loose layer movement angle, the uphill movement angle, the downhill movement angle, and the sampling depth of the working surface boundary: as follows:

$$L_{rise} = h\cot\varphi + (H_{rise} - h)\cot(\gamma - \Delta\gamma) \quad (2)$$

$$L_{dip} = h\cot\varphi + (H_{\mathrm{dip}} - h)\cot(\beta - \Delta\beta) \quad (3)$$

In the above equations (2) and (3), H_{rise} is the mining depth in the mountain direction, H_{dip} is the mining depth in the descending direction of the working face; γ is the uphill movement angle; β is the downhill movement angle; $\triangle\gamma$ is the correction value of uphill movement angle; and $\triangle\beta$ refers to the correction value of downhill movement angle.

(2) Measurement at the mobile observation stations

The connected measurement, comprehensive measurement, and daily observation [26] are combined in the mobile observation stations in this study. The specific contents are given as follows. Firstly, the connected measurement is based on the ground control network of the Tingnan mining area to study the observation line control point K02, which is connected with the points E10 and E19 in the mining control network, so that the coordinates and elevation of the control point K02 can be measured. E-class global position system (GPS) adopted for control point contact measurement. The technical requirements are shown in the Table 2 below.

Table 2: Technical requirements of the observation station

Type	Value
Fixed error (mm)	≤ 10
Percentage error coefficient (10-6)	≤ 10
The number of edges of a closed ring	≤ 10
Mean distance (km)	0.2 - 5
Number of synchronous receivers	≥ 2
The length of the time	≥ 40 minutes
Number of observation periods	≥ 1.6
Satellite cutoff altitude Angle	15°
Number of observation satellites	≥ 4
Maximum PDOP value	≤ 6

Note: PDOP in the table refers to position dilution of precision; the relative median error of the baseline edge length should not exceed $\delta=\sqrt{(10\mathrm{mm})^2+(10\mathrm{ppm}\cdot\mathrm{s})^2}$; the closing error of the coordinate component of the synchronization ring and the total length of the closing error are not less than 6 ppm and 10 ppm, respectively; the length of retest baseline is not less than $2\sqrt{2}\delta$; the relative mean error of the weakest side is not less than 1/20000.

Due to the influence of the topographical factors of the research area, the static GPS is combined with the total station to attach the traverse measurement method. That is, 4 ~ 10 points are selected on each observation line as GPS points, which can form a GPS network with the control points in the observation station, so as to measure according to the E-level GPS accuracy requirements [27]. On this basis, the GPS point is undertaken as the starting point of the traverse, and the attached traverse is laid along the observation line according to the requirements of the 5-second traverse, and the plane coordinates of each point are measured. The four-level leveling is adopted for round-trip observations of the elevation, and individual survey points with complex terrain can be measured using total station trigonometric elevation.

The comprehensive observation is carried out independently after the connected measurement and before the surface movement, and the time interval between the two observations is not more than 4 days. When the elevation difference of the same point between these two measurements is ≤ 10 mm, the offset is the same ≤ 30 mm, and the same side length is the same ≤ 4 mm, the average value can be used as the original data. If a total station and GPS are adopted for observation, it can be converted according to the coordinates of the observation data as a criterion. While if the geometric leveling is applied to observe the elevation of each measuring point, dynamic GPS can be applied to observe the plane coordinate changes of each measuring point. In each comprehensive observation, two independent measurements are taken at different time intervals, and each observation is set with 3 coordinate readings. When the coordinate difference between the average results of the two observations exceeds 20 mm, it should be re-observed with the static GPS method or the total station.

II. D. Data simulation technology

The UDEC is adopted in this experiment. UDEC is a discrete element method based on a wide range of applications in various industries such as mining, petroleum, and civil engineering [28], [29]. It is mainly used to simulate the numerical analysis of discontinuous systems and is the preferred analysis program for continuous rock mechanics and structure matters [30]. UDEC can simulate the movement and rotation of rocks in space, and can realize full

model simulation in engineering design. Compared with continuous deformation calculation software such as FLAC3D, UDEC can more truly reflect the movement of the overlying rock and ground [31].

In the research of coal mining related fields, the UDEC software is suitable for the study of surface movement under the conditions of large-area mining with multiple working faces, which can reflect the subtle influence of section coal pillars on the ground surface, so it is in line with the design requirements of this research [32], [33]. Therefore, it is adopted in this study.

The Mohr-Coulomb constitutive model is undertaken as the reference model. The overlying rock layers with similar lithology or thinner thickness are combined into one layer, so as to simplify the model and facilitate the calculation. The description of pore lithology is easy to subdivide into multiple small layers [34]. The effect of using UDEC to establish a two-dimensional numerical calculation model is shown in Figure 1 below. The entire model is composed of 18,820 units, and the model size can be derived from the coordinates in the figure.

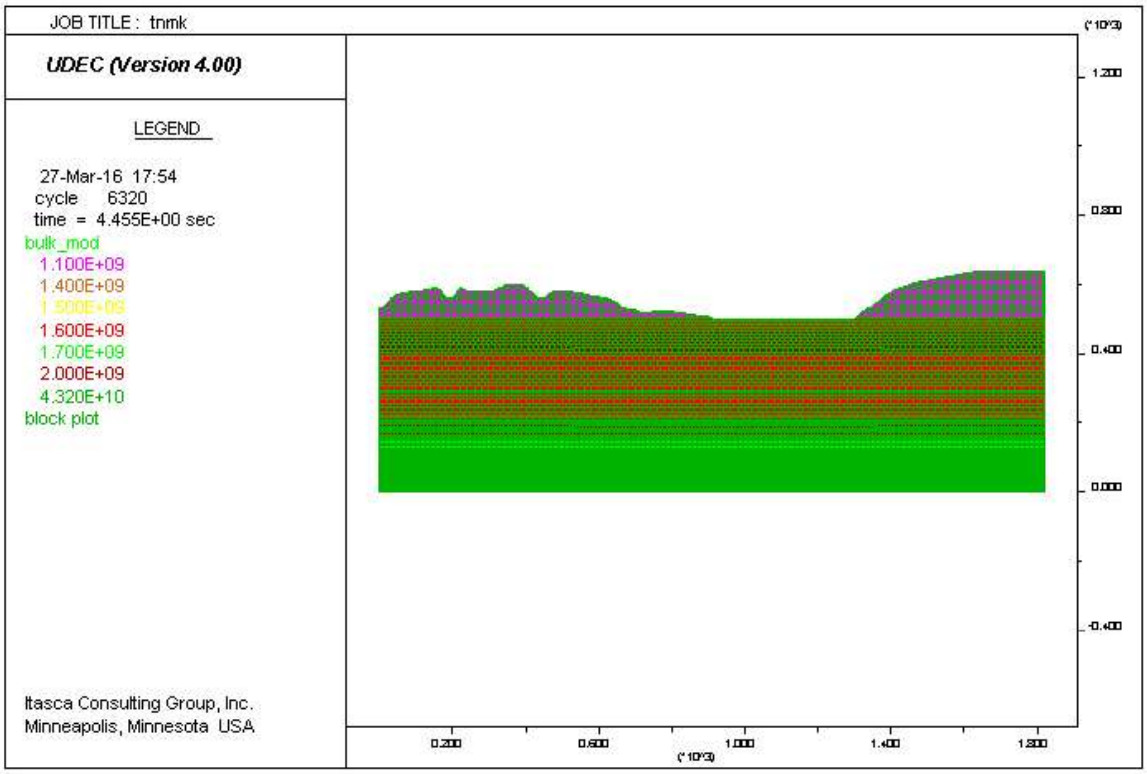

Figure 1: Two-dimensional calculation model of UDEC

III. Results and discussion

III. A. Observation results for surface movement of targeted working area

Parameters for surface movement after mining the 204 working area are shown in Table 3 below, which are obtained based on the analysis of observation data in the line B.

Table 3: Parameters for surface movement of 204 working surface

Type	Value
Inclined range (L/H)	0.29 ~ 0.42
Subsidence rate (q)	0.046
Horizontal movement coefficient (b)	0.337
Boundary angle ($\delta 0$)	57.1°
Movement angle (δ)	/
Crack angle (δ'')	84.4°

Table 3 indicates that the maximum subsidence value w_{max} = 246 mm and the subsidence rate q' = 0.046. Maximum horizontal movement value u_{max} = 83 mm and the horizontal movement coefficient b = 0.337. Since the movement deformation value of the inclined main section after the mining of 204 working face is very small, it

is necessary to judge the comprehensive movement situation according to the critical deformation value. The deformation parameters include: inclined i = ± 3.0 mm/m, curvature ε = ± 2.0 mm/m, and horizontal deformation value K = ± 0.2×10-3/m. The curves of the three parameters are shown in Figure 2 below.

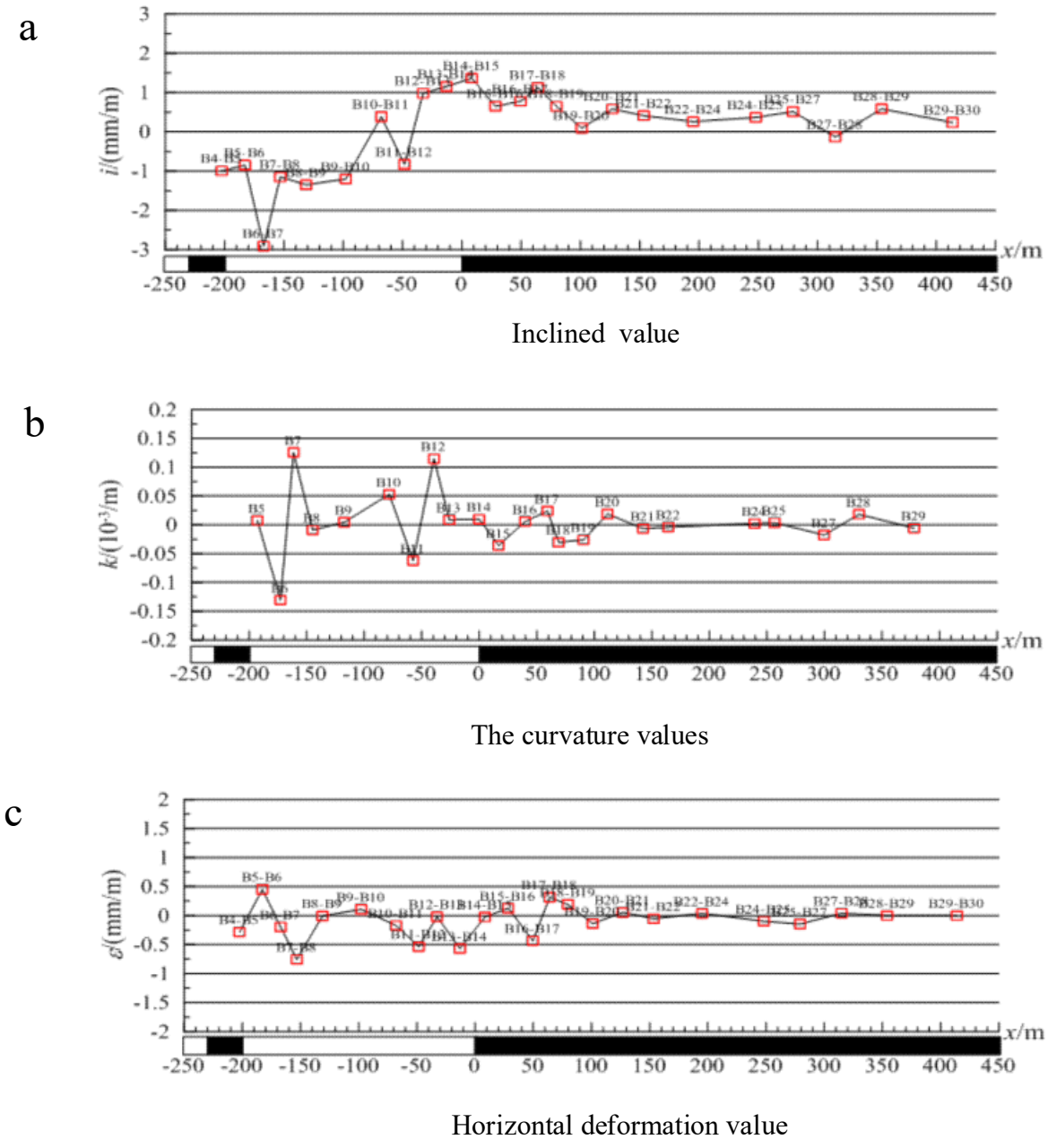

Figure 2: Parameters of critical deformation values in 204 working area

The distribution law of subsidence and horizontal movement in working area 205 is shown in Figure 3. It illustrates that the maximum surface subsidence is 1,177 mm, located at point B6, which is -172.7 meters away from the mining boundary, and the subsidence rate q' = 0.22. The maximum horizontal movement value of the surface reaches -687.2 mm, which is located at point B13, -26m from the mining boundary, and the horizontal movement coefficient b = 0.58.

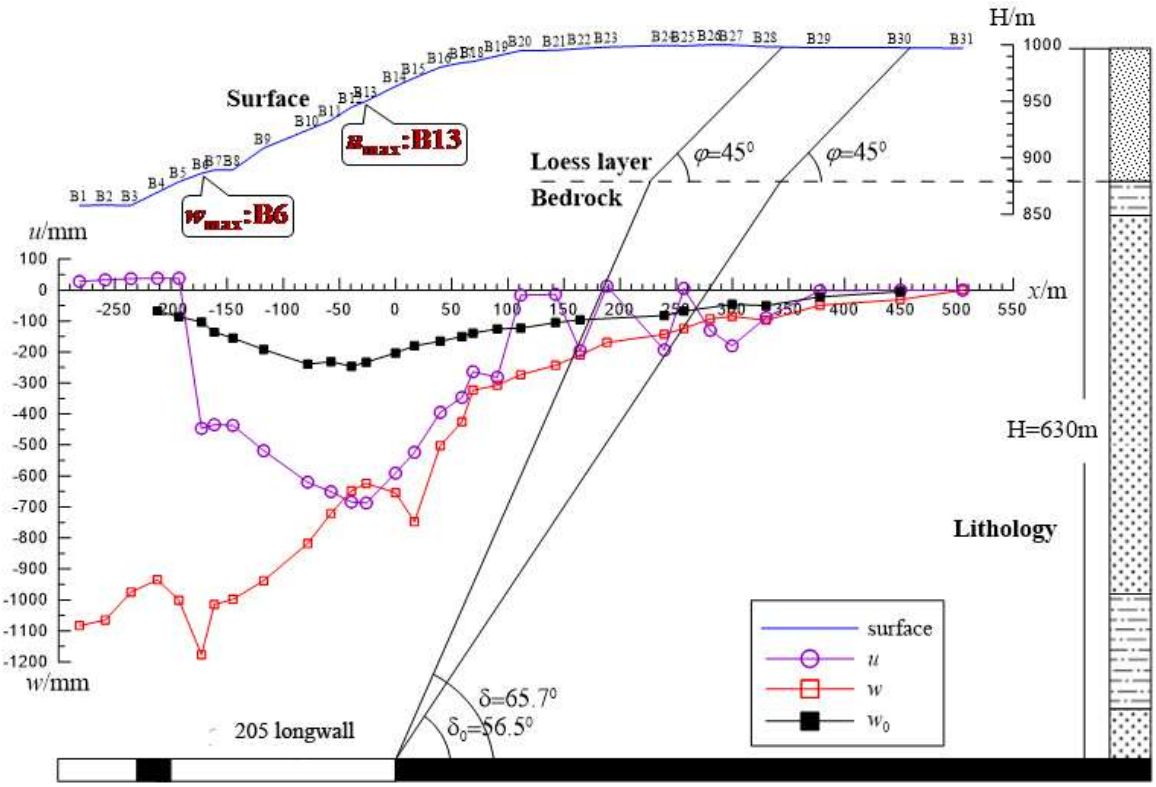

Figure 3: The distribution law of subsidence and horizontal movement in surface observation points of observation line in the working area 205

Table 4 shows the surface movement parameters for mining of working surface 205, as follows:

Table 4: Surface movement parameters of working surface 205

Type	Value
Inclined range (L/H)	0.62 ~ 0.91
Subsidence rate (q')	0.22
Horizontal movement coefficient (b)	0.58
Boundary angle ($\delta 0$)	54.11°
Movement angle (δ)	61.12°
Crack angle (δ'')	84.4°

It is known that the ratio of mining width to mining depth is 0.62 ~ 0.91, which is greater than 1/3, closing to 1.2 ~ 1.4 of the judgment condition of full mining. The surface subsidence rate has increased significantly, but the value is only 0.22, which belongs to insufficient mining close to the conditions of full mining. The surface deformation is obvious, and the comprehensive movement angle reaches 61.12°. The surface deformation and damage are still small, no new surface cracks are generated, the crack angle is still 84.4°, and the loess gully slope is stable. Inclined I = ± 3.0 mm/m; curvature ε = ± 2.0 mm/m; and horizontal deformation value K = ± 0.2×10-3/m. The curves of the three parameters are shown in Figure 4.

III. B. Analysis on data simulation results

Figure 5a shows the overlying rock and surface subsidence cloud map after mining the 204 working surface, and Figure 5b shows the partial enlarged subsidence cloud map of the center of the surface subsidence basin of 204 working surface. Figure 5a suggests that the surface subsidence on the slope directly above the 204 working face is relatively large, the maximum surface subsidence is in the range of 200 ~ 800 mm, and the surface subsidence in other areas is within 200 mm. Figure 5b reveals that the maximum surface subsidence is in the range of 300 ~ 400 mm. The point of maximum surface subsidence is located at the lower part of the larger part of the slope angle, near the center of the mining area. Affected by surface slippage, the surface subsidence value in mountainous areas is larger than that of the horizontal surface. The maximum surface subsidence value is not in the center of the mining area, but on the nearby slopes with larger slippage.

a

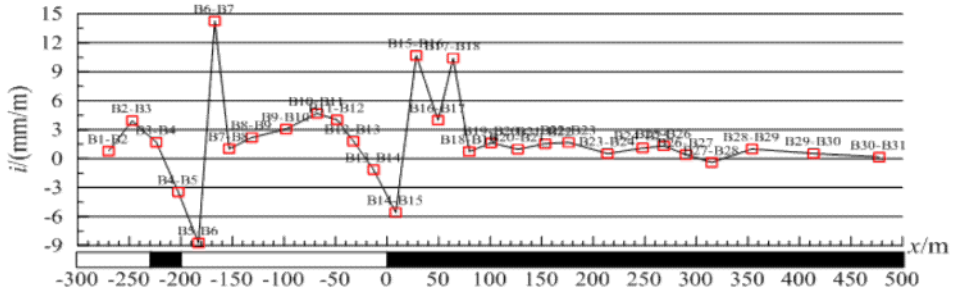

Inclined value

b

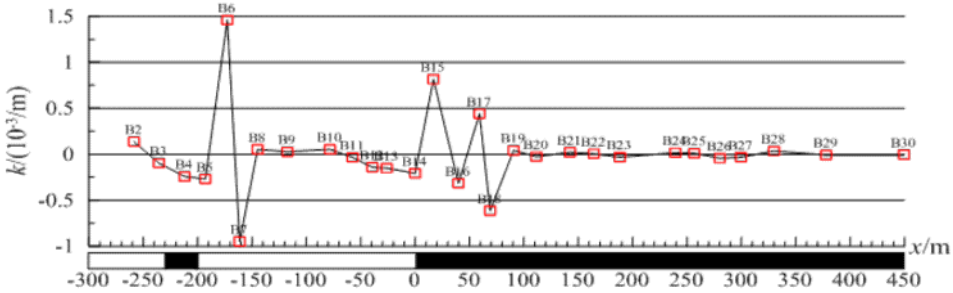

The curvature values

c

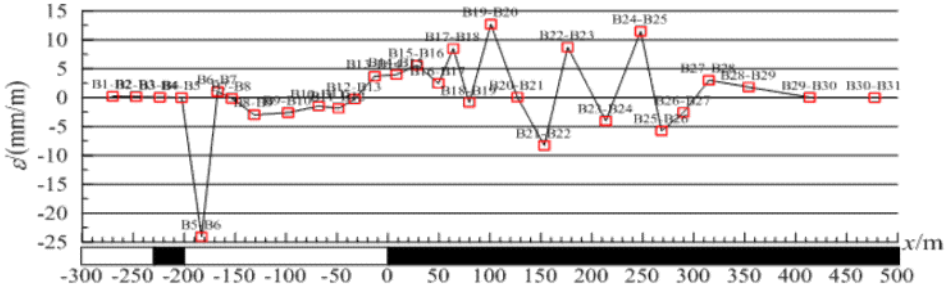

Horizontal deformation value

Figure 4: Parameters of critical deformation values in 205 working area

a

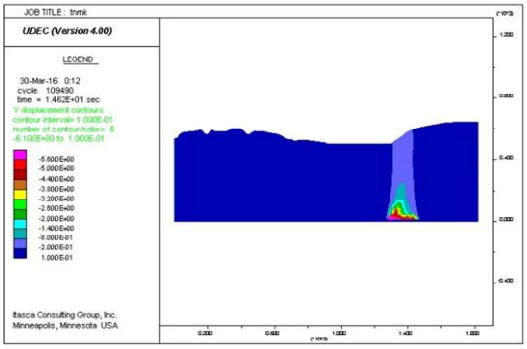

b

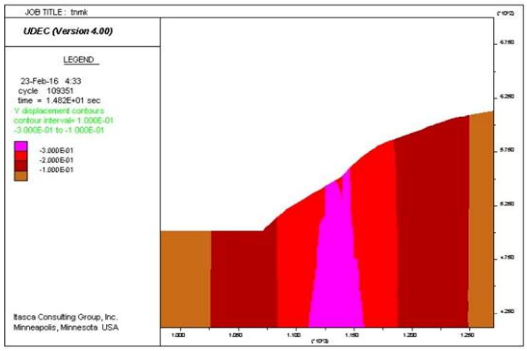

Figure 5: Surface subsidence cloud map of working area 204

Figure 6a shows the overlying rock and ground subsidence cloud map after mining at 205 working face, and Figure 6b is a partially enlarged subsidence cloud map of the center of the surface subsidence basin. Figure 6a suggests that the maximum surface subsidence point is not on the surface above the center of the mining area, but on the slope above the 204 working face, which is close to the coal pillar side affected by the slope slip and the section coal pillar support; and the largest surface subsidence value is 1,300 ~ 1,900 mm. Figure 6b indicates that the maximum surface subsidence is 1,300~1,500 mm.

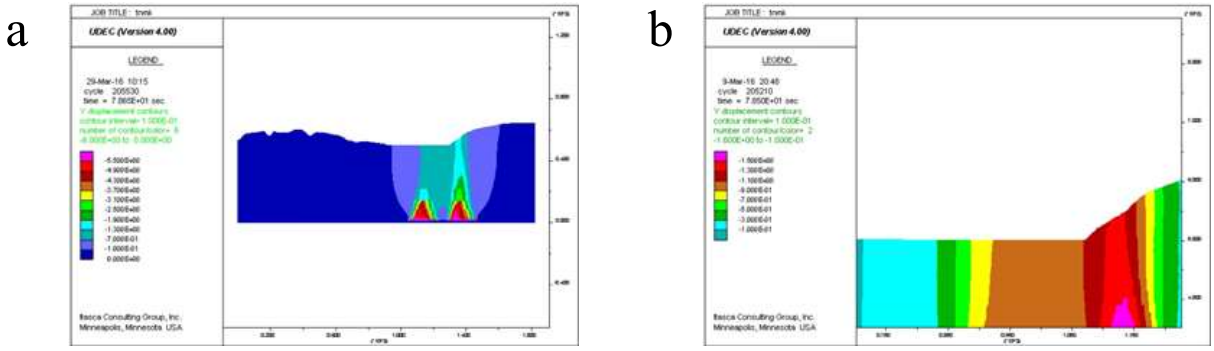

Figure 6: Surface subsidence cloud map of working area 205

III. C. Comparison between predicted value and measured value

The simulated values are compared with the measured values, and the following results are obtained. As shown in Figure 7, the simulated surface subsidence curve shows that after the mining of 204 working face, the maximum surface subsidence value is 270 mm, and the subsidence rate is 0.045, which is the same as the measured value basically. After mining the 205 working face, the maximum surface subsidence is 1,205 mm, and the subsidence rate is 0.201. Affected by the section coal pillar a and the surface slope, the maximum subsidence point is located above the coal pillar on the side of the 204 working face, which is consistent with the measured value basically.

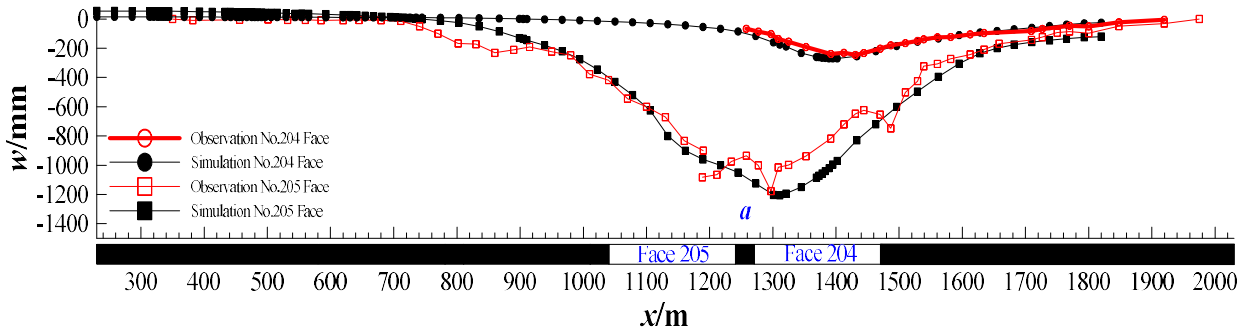

Figure 7: Comparison on measured values and simulated values

Figure 8a shows that after mining the 204 working face, the maximum horizontal movement value of the surface is -88 mm, and the horizontal movement coefficient is 0.326, which is basically consistent with the measured value. Figure 8b suggests that after 205 working face is mined, the maximum horizontal movement value of the ground surface is -699 mm, and the horizontal movement coefficient is 0.58, which is basically consistent with the measured value. Affected by the section coal pillar a, the simulated horizontal movement value rebounds slightly at the coal pillar.

The measured and simulated values for subsidence and horizontal movement curves of the working area 204 and 205 are compared, and the results show that the selected model and the parameters used in the model can basically reflect the actual field observations, and can be undertaken as a basis for the subsequent mining of the model. The surface movement law obtained by simulation after mining has reference value.

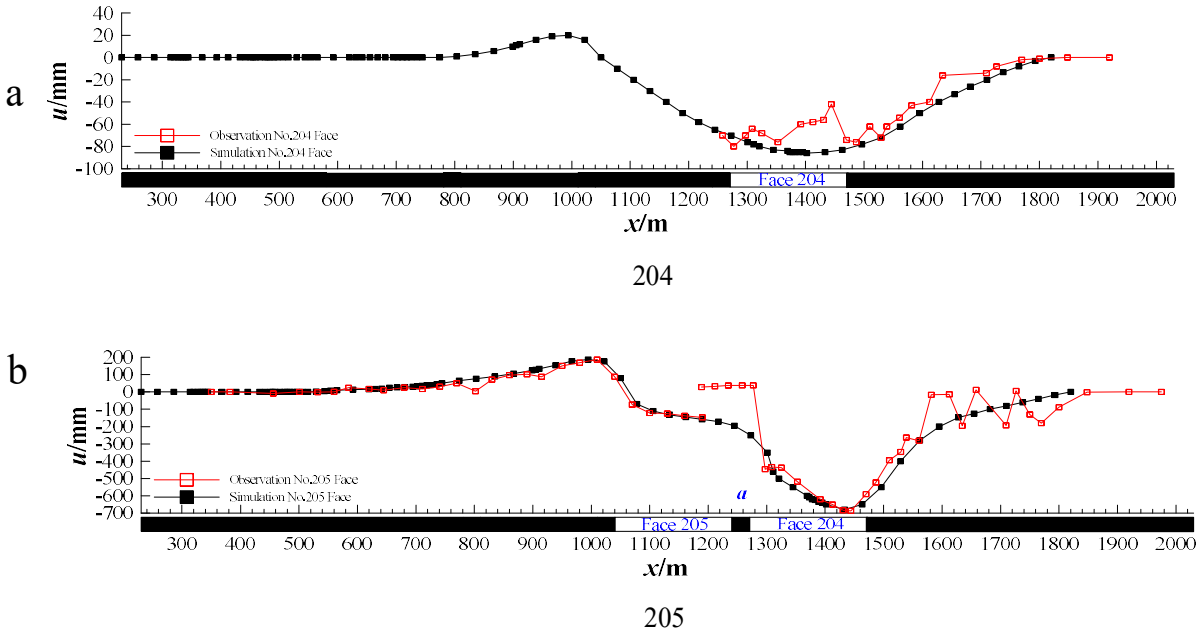

Figure 8: Comparison on simulated values and measured values of surface movement in working area 204 and 205

IV. Conclusion

Based on the movement observation technology and numerical simulation technology, the surface movements of the 204 and 205 working areas are explored fully, and the surface movement parameters are obtained finally. The specific results are as follows: the maximum surface subsidence value of the 204 working surface is 246 mm with the subsidence rate q' of 0.046, the maximum horizontal movement value is 83 mm, and the horizontal movement coefficient is 0.337. The deformation parameters include inclined of ± 3.0 mm/m, curvature of ± 2.0 mm/m, and horizontal deformation value of ± 0.2×10-3/m. Compared with the 204 working area, the subsidence rate of the 205 working area is greatly increased, but the data is only 0.22, indicating that it belongs to the inadequate mining close to the sufficient mining conditions. In addition, the surface deformation in working area 205 is obvious, and the comprehensive movement angle reaches 61.12°. The result of data simulation shows that the result of numerical simulation is basically consistent with the measured values, and the effect of data simulation is relatively good.

References

[1] Feng Y, Wang J, Bai Z, et al. Effects of surface coal mining and land reclamation on soil properties: A review. Earth-science reviews, 2019, 191, pp. 12-25.

[2] Xu C, Nie W, Liu Z, et al. Multi-factor numerical simulation study on spray dust suppression device in coal mining process. Energy, 2019, 182, pp. 544-558.

[3] Ye Q, Wang G, Jia Z, et al. Similarity simulation of mining-crack-evolution characteristics of overburden strata in deep coal mining with large dip. Journal of petroleum science and engineering, 2018, 165, pp. 477-487.

[4] Xie H, Gao M, Zhang R, et al. Study on the mechanical properties and mechanical response of coal mining at 1000 m or deeper. Rock mechanics and rock engineering, 2019, 52(5), pp. 1475-1490.

[5] Oei P Y, Brauers H, Herpich P. Lessons from Germany's hard coal mining phase-out: policies and transition from 1950 to 2018. Climate policy, 2020, 20(8), pp. 963-979.

[6] Qiao W, Li W, Li T, et al. Effects of coal mining on shallow water resources in semiarid regions: a case study in the Shennan mining area, Shaanxi, China. Mine water and the environment, 2017, 36(1), pp. 104-113.

[7] Wang J, Zhou G, Wei X, et al. Experimental characterization of multi-nozzle atomization interference for dust reduction between hydraulic supports at a fully mechanized coal mining face. Environmental science and pollution research, 2019, 26(10), pp. 10023-10036.

[8] Scott B, Ranjith P G, Choi S K, et al. A review on existing opencast coal mining methods within Australia. Journal of mining science, 2010, 46(3), pp. 280-297.

[9] Liu S, Li W, Wang Q. Zoning method for environmental engineering geological patterns in underground coal mining areas. Science of the total environment, 2018, 634, pp. 1064-1076.

[10] Sun Q, Zhang J, Qi W, et al. Backfill mining alternatives and strategies for mitigating shallow coal mining hazards in the western mining area of China. quarterly journal of engineering geology and hydrogeology, 2020, 53(2), pp. 217-226.

[11] Sidorenko S A, Ivanov V V. Improving the efficiency underground mining of coal beds in difficult mining and geological conditions. ARPN journal of engineering and applied sciences, 2017, 12(3), pp. 882-888.

[12] Yang Z, Li W, Pei Y, et al. Classification of the type of eco-geological environment of a coal mine district: A case study of an ecologically fragile region in Western China. Journal of cleaner production, 2018, 174, pp. 1513-1526.

[13] Litvin O, Tyulenev M, Zhironkin S, et al. Methodology of coal losses calculation at open pit mining for complex geological conditions–review. Acta montanistica slovaca, 2017, 22(2), pp. 146-152.
[14] Ooriad F A, Yari M, Bagherpour R, et al. The development of a novel model for mining method selection in a fuzzy environment; case study: Tazareh Coal Mine, Semnan Province, Iran. Rudarsko-geološko-naftni zbornik, 2018, 33(1), pp. 45-53.
[15] Liu S, Li W, Wang Q, et al. Water inrush risk zoning and water conservation mining technology in the Shennan mining area, Shaanxi, China. Arabian journal for science and engineering, 2018, 43(1), pp. 321-333.
[16] Wang Y, Liang B, Yuan X. Study on safety mining method of fully-mechanized top-coal caving in coal seam with easy spontaneous combustion and high coal dust. Journal of mining & safety engineering, 2012, (5), pp. 23.
[17] Li S G, Lin H F, Zhao P X, et al. Dynamic evolution of mining fissure elliptic paraboloid zone and extraction coal and gas. Journal of china coal society, 2014, 39(8), pp. 1455-1462.
[18] Xia Y, Tang J, Meng X. Study on distribution regularity of coal-body gas pressure near coal draw-point in early stage of caving mining. Mining safety & environmental protection, 2009, (1), pp. 4.
[19] Lei C, Guan Y. Comparatine analysis of ground collapse the caused by coal mining. The Chinese journal of geological hazard and control, 2011, (3), pp. 11.
[20] Wang G, Zhao Z, Ning Y. Design of compressed sensing algorithm for coal mine IoT moving measurement data based on a multi-hop network and total variation. Sensors, 2018, 18(6), pp. 1732.
[21] Li J, Xu Z. Research on network layout strategy of mobile opportunity perception in coal mines. International journal of computational science and engineering, 2020, 22(1), pp. 124-134.
[22] Feng X, Li Q, Tao Y, et al. Impact of coal replacing project on atmospheric fine aerosol nitrate loading and formation pathways in urban Tianjin: Insights from chemical composition and 15N and 18O isotope ratios. Science of the total environment, 2020, 708, pp. 134797.
[23] Li M G, Zhu H, You S Z, et al. UWB-based localization system aided with inertial sensor for underground coal mine applications. IEEE sensors journal, 2020, 20(12), pp. 6652-6669.
[24] Zhang J, Zhang Q, Sun Q, et al. Surface subsidence control theory and application to backfill coal mining technology. Environmental earth sciences, 2015, 74(2), pp. 1439-1448.
[25] Zhang B, Zhao W, Wang W, et al. Pressure characteristics and dynamic response of coal mine refuge chamber with underground gas explosion. Journal of loss prevention in the process industries, 2014, 30, pp. 37-46.
[26] Wang J, Yu B, Kang H, et al. Key technologies and equipment for a fully mechanized top-coal caving operation with a large mining height at ultra-thick coal seams. International journal of coal science & technology, 2015, 2(2), pp. 97-161.
[27] Zheng M, Li X, Liu J, et al. Pyrolysis of Liulin coal simulated by GPU-based ReaxFF MD with cheminformatics analysis. Energy & fuels, 2014, 28(1), pp. 522-534.
[28] Gao F, Stead D, Coggan J. Evaluation of coal longwall caving characteristics using an innovative UDEC Trigon approach. Computers and geotechnics, 2014, 55, pp. 448-460.
[29] Gao F, Stead D, Kang H. Simulation of roof shear failure in coal mine roadways using an innovative UDEC Trigon approach. Computers and geotechnics, 2014, 61, pp. 33-41.
[30] Yao Q, Li X, Sun B, et al. Numerical investigation of the effects of coal seam dip angle on coal wall stability. International journal of rock mechanics and mining sciences, 2017, 100, pp. 298-309.
[31] Ying-Ke L, Fu-Bao Z, Lang L, et al. An experimental and numerical investigation on the deformation of overlying coal seams above double-seam extraction for controlling coal mine methane emissions. International journal of coal geology, 2011, 87(2), pp. 139-149.
[32] Bai Q S, Tu S H, Zhang C, et al. Discrete element modeling of progressive failure in a wide coal roadway from water-rich roofs. International journal of coal geology, 2016, 167, pp. 215-229.
[33] Wu B, Wang X, Bai J, et al. Study on crack evolution mechanism of roadside backfill body in gob-side entry retaining based on UDEC trigon model. Rock mechanics and rock engineering, 2019, 52(9), pp. 3385-3399.
[34] Vakili A, Hebblewhite B K. A new cavability assessment criterion for longwall top coal caving. International journal of rock mechanics and mining sciences, 2010, 47(8), pp.1317-1329.